Axial-Strain-Induced Torsion in Single-Walled Carbon Nanotubes

Haiyi Liang and Moneesh Upmanyu*

Group for Simulation and Theory of Atomic-Scale Material Phenomena (stAMP) Materials Science Program, Division of Engineering, Colorado School of Mines, Golden, Colorado 80401, USA

(Received 17 May 2005; published 25 April 2006)

Using classical molecular dynamics and empirical potentials, we show that the axial deformation of single-walled carbon nanotubes is coupled to their torsion. The axial-strain-induced torsion is limited to chiral nanotubes—graphite sheets rolled around an axis that breaks its symmetry. Small strain behavior is consistent with chirality and curvature-induced elastic anisotropy (CCIEA)—carbon nanotube rotation is equal and opposite in tension and compression, and decreases with curvature and chirality. The large-strain compressive response is remarkably different. The coupling progressively decreases, in contrast to the tensile case, and changes its sign at a critical compressive strain. Thereafter, it untwists with increasing axial strain and then rotates in the opposite direction, i.e., the same sense as under tension. This suggests that the response is now dictated by a combination of nonlinear elasticity and CCIEA.

DOI: 10.1103/PhysRevLett.96.165501 PACS numbers: 62.25.+g, 62.20.Dc, 81.07.De, 85.85.+j

The combination of high stiffness, low density, and structural specificity of carbon nanotubes has motivated several studies aimed at understanding their electronic, thermal and mechanical properties. The development of efficient fabrication routes for single- and multiwalled carbon nanotubes (SWCNTs and MWCNTs) and their bundles have accelerated their use as nanoscale building blocks in field-emission displays, electrochemical energy storage, interconnects, supercapacitors, and nanotransistors, with potential applications in nanoelectronics, nanocomposites, drug delivery systems, and biochemical sensors [1]. Electromechanical couplings inherent in CNTs are the basis for the rapid shift towards CNT-based nanoelectromechanical systems (CNT-NEMS) [1–3]. For example, the large electromechanical response in SWCNTs ($\sim$1%) can be harnessed to fabricate actuators and switches for electronic circuits and devices [4,5]. Doubly clamped MWCNTs have been recently used as rotational springs and bearings to fabricate paddle oscillators and nanomotors [6,7], wherein the MWCNT transfers its rotational degree of freedom to an electrostatically actuated metal plate rigidly patterned onto its outer shell. Electrostatically actuated transverse vibrations have also been realized, quite like a plucked guitar string. The response is tunable, and can be used to fabricate self-detecting, high frequency mechanical resonance oscillators [8].

In most CNT-NEMS applications, the possibility of mechanical couplings is ignored. Here, our focus is on axial-strain-induced torsion (a-SIT) in SWCNTs. The a-SIT response can modify electronic, thermal, and mechanical properties of CNTs, underscoring its importance in CNT-NEMS devices that exploit electro-, thermo-, chemico-, and optico-mechanical response of CNTs. For example, torques produced in MWCNT-based rotational bearings, oscillators, and nanomotor shafts can result in axial strains that can modify the oscillatory response. Conversely, axial strains generated during transverse vibrations of SWCNTs can result in torsional strains which not only affect the predicted resonant frequencies of the SWCNTs, but can also change their electronic properties.

Recently, Gartestein *et al.* employed a 2D continuum model to describe a-SIT in CNTs [9]. For small strains and curvatures, they predict that the induced torsion is limited to chiral CNTs, i.e., when the CNT axis (or chiral vector C_h) does not coincide with the basis vectors of the underlying sixfold symmetric graphite lattice. Note that the chiral vector is a linear combination of the graphite basis vectors $\mathbf{a}_1$ and $\mathbf{a}_2$, i.e., $C_h = n\mathbf{a}_1 + m\mathbf{a}_2$ (n and m are integers), and the chiral angle θ (the angle between the chiral vector C_h and the nearest basis vector) lies between 0° and 30°. The authors conclude that a-SIT is a maximum for $\theta = \pi/12$ chiral nanotubes. General scalings laws are then used to predict the chirality and curvature dependence of a-SIT in SWCNTs. Given the small strain limitation of the continuum model, it is important to understand the a-SIT response for typical SWCNT (radius $R \leq 20$ Å) and using atomic-scale techniques.

Here, we perform classical molecular dynamics (MD) simulations of finite length SWCNTs subject to an axial strain ϵ. We systematically investigate the a-SIT response as a function of SWCNT structure, mainly CNT curvature κ and chirality (n, m). The simulations are performed for strains $\epsilon \sim 5\%$ in tension, and till buckling under compression, i.e., $\epsilon \sim 10\%$. The computational cell is shown in Fig. 1 (inset, top left). The aspect ratio of each simulated SWCNTs is $\sim$4. We have verified that this length is sufficient to eliminate size-effect related artifacts. The second generation reactive empirical bond order (REBO) potential is employed to describe the carbon-carbon interactions [10]. Our choice is motivated by the fact that the potential is based on accurate analytic functions for carbon-carbon interactions (bond energies, lengths, and angles), and the large fitting base accurately reproduces elastic properties of diamond and graphite. For effective

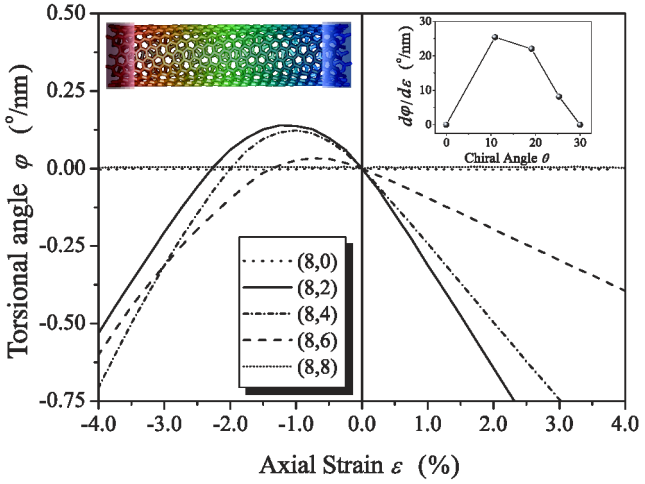

FIG. 1 (color online). Chirality dependence of the a-SIT response for $(8, m)$ SWCNTs. (inset, top left) Atomic-plot of the simulation cell depicting a chiral $(8, 4)$ SWCNT subject to an axial strain (in this case, compression). Color indicates the atomic distribution of the twist ϕ about the CNT axis with respect to the unstrained case. (inset, top right) Chirality dependence of zero-strain coupling, $d\phi/d\epsilon|_{\epsilon=0}$.

comparison with theory, all simulations are performed at 10^{-3} K using a Langevin thermal bath. As-constructed SWCNTs are first subject to an equilibration simulation for 50 ps, and then strained by prescribing *axial* displacements of end atoms (masked in the figure). Each end portion is 0.6 nm wide. The end atoms are not rigidly clamped; they are allowed to relax both radially and tangentially during deformation. Each prescribed displacement step results in an axial strain $|\epsilon| = 0.25\%$, and is followed by long relaxation of 50 ps (strain rate $|\dot{\epsilon}| = 5 \times 10^7\ \mathrm{s}^{-1}$). The reported torsional angle ϕ is the relative twist per unit length between corresponding segments of the two ends of the SWNT.

In order to determine the effect of chirality, we have investigated the a-SIT response in $(8, m)$ SWCNTs, for $m = 0, 2, 4, 6, 8$. Axial strain dependence of the induced torsion angle ϕ is plotted in Fig. 1. The a-SIT response is negligible in the two achiral SWCNTs. On the other hand, the three chiral SWCNTs are torsionally strained under both compression and tension. The twist distribution antisymmetric across its ends, as shown in Fig. 1 (inset, top left). From these results, we conclude that the a-SIT response is limited to chiral SWCNTs. At small strains, the twist is antisymmetric in tension and compression and varies linearly with strain, approaching $0.25°/\mathrm{nm}$ at $\epsilon = 1\%$ for the $(8, 2)$ SWCNT. At large tensile strains, ϕ continues to increase (almost linearly) with strain. For the $(8, 2)$ and $(8, 4)$ SWCNTs, $\phi \sim 1°/\mathrm{nm}$ at strains $\epsilon = 4\%$. In typical NEMS applications, where SWCNTs can extend to close to 1 μm, our results show that even the small strain a-SIT ($|\epsilon| \leq 1\%$) can (relatively) twist the CNT ends by almost 250°. Interestingly, the behavior under compression is qualitatively different. While the magnitude of ϕ still increases with strain, the unit length coupling $d\phi/d\epsilon$ decreases. At a critical value ϵ_1^*, $d\phi/d\epsilon = 0$. It then changes sign and increases again. In effect, the SWCNT untwists and at another critical strain ϵ_2^* the twist is completely eliminated ($\phi = 0$). Upon further compression, the SWCNT starts to twist in the opposite direction, i.e., in the same direction as in tension. The anharmonicity under compression suggests that the a-SIT response is qualitatively different at large compressive strains.

We now pause to investigate the small strain response in greater detail. While our results clearly demonstrate that chirality is necessary for the a-SIT response, the $(8, 2)$ SWCNT exhibits a larger coupling than the $(8, 4)$ case although their chiral deviation from $\pi/12$ is almost the same (Fig. 1, top right). This trend is also observed at large-strains—the coupling, critical compressive strains (ϵ_1^*, ϵ_2^*) and extremum in the induced torsional angle are all greater for the $(8, 2)$ SWCNT. One exception is the coupling at large compressive strains, where the $(8, 4)$ response is greater than the $(8, 2)$ case. To isolate the effect of tube curvature, we have performed simulations for a series of $(n, n/2)$ SWCNTs. The chiral angle is now fixed while the tube curvature varies inversely with n. Figure 2(a) shows the a-SIT response for $n = 6, 8, 12, 20$. In each case, the overall behavior is similar to that observed for $(8, m)$ chiral SWCNTs (Fig. 1). The curvature dependence is shown in Fig. 2(b), a plot of $d\phi/d\epsilon|_{\epsilon=0}$ vs κ^{-1}. The decrease is monotonic and can be described by a polynomial fit, i.e.,

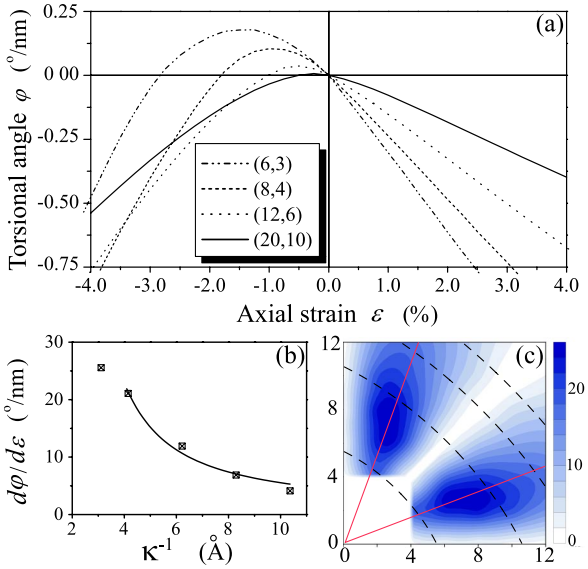

FIG. 2 (color online). Curvature dependence of the (a) a-SIT response for $n, n/2$ chiral SWCNTs, and (b) the zero-strain coupling, $d\phi/d\epsilon|_{\epsilon=0}$. The curve fit in (b) is of the form $(a\kappa + b\kappa^3 + \cdots)$. (c) Chirality-curvature contour map of the coupling in (n, m) SWCNTs, $6 \geq n$, $m \geq 12$. The scale bar is in units of °/nm. Dashed lines correspond to constant curvature, while $\theta = \pi/12$ chirality is shown as solid lines.

$d\phi/d\epsilon = (a\kappa + b\kappa^3 + \cdots)$, with $a = 48.5$ Å and $b = 687.1$ Å^3 [11]. Note that the continuum model predicts a κ^3 leading order dependence. The large-strain curvature dependence also decreases with curvature—the coupling, extrema in twist $\phi(\epsilon_1^*)$ and critical strains (ϵ_1^*, ϵ_2^*) decrease with curvature. The curvature dependence at high strains ($\epsilon = 4\%$, not shown) reveal that the decay is again dominated by terms linear and cubic in κ. The fact that the progressive weakening of a-SIT at high strains is of the same order in curvature as that at zero strain strongly suggests that (i) the chirality- and curvature-induced elastic anisotropy (CCIEA) results in a-SIT, and that (ii) we expect the a-SIT response of CNTs to be always anharmonic in compression.

Clearly, the a-SIT in (8, 2) SWCNT is larger compared to that in the (8, 4) SWCNT due to its higher curvature. This is also evident from the chirality-curvature contour map [Fig. 2(c)] of the zero-strain coupling $d\phi/d\epsilon|_{\epsilon=0}$ for several (n, m) SWCNTs ($4 \leq n, m \leq 12$). As expected, the coupling is negligible for both armchair (n, n) and zigzag $(n, 0)$ SWCNTs. The combined effect of chirality and curvature results in the maximum coupling for (8, 2) and neighboring SWCNTs, i.e., $d\phi/d\epsilon \sim 25°/\text{nm}$. However, for SWCNTs with comparable radii (dotted lines), the largest coupling is midway between armchair and zigzag nanotubes, for chiral angles close to $\pi/12$ (solid lines).

As a first step towards understanding the a-SIT due to curvature and chirality induced elastic anisotropy (CCEIA), we develop a simple continuum model for the small strain response. The axially strained CNT is coupled to its twist via anisotropy in its mechanical energy (per unit length), i.e., $\mathcal{F}(\epsilon, \phi) \neq \mathcal{F}(\epsilon, -\phi)$. The energy functional that captured a-SIT takes the form [12]:

$$\mathcal{F} \approx \delta E_b + \frac{1}{2}[k_e\epsilon^2 + k_t\phi^2 + 2k_{et}\phi\epsilon + \cdots] - F\epsilon,$$

where δE_b is the contribution due to coupling between axial strain and curvature (Poisson's effect), k_e and k_t are the extensional and torsional rigidities, F is the axial force exerted on the SWCNT and k_{et} is the constant that couples axial strain to twist. Additional couplings between (axial and torsional) strains and curvature are captured implicitly via the curvature dependence of the coupling constant, κ_{et}. Minimizing $\mathcal{F}$ at a force controlled strain $[\partial\mathcal{F}/\partial\epsilon = 0]$ yields the equilibrium twist and therefore the coupling, $d\phi/d\epsilon = -k_{et}/k_t$. For the range of SWCNTs studied here, the variation in k_t is quite small [13]. Hence, the a-SIT response is primarily due to the coupling constant, i.e., $k_{et} \equiv k_{et}(\kappa, \theta)$. It is reasonable to decouple the curvature and chirality dependencies as $k_{et}(\theta, \kappa) = f(\theta)g(\kappa)$, where $f(\theta)$ and $g(\kappa)$ capture the leading order variations. The curvature dependence follows from our results for $(n, n/2)$ SWCNTs [Fig. 2(b)], i.e., $g(\kappa) = (a\kappa + b\kappa^3 + \cdots)$. Symmetry arguments based on harmonic deformations on a hexagonal background dictate that $f(\theta) \propto \sin 6\theta$. Then, the coupling is a maximum for $\theta = \pi/12$ chirality SWCNTs.

Returning to the curvature dependence, the coupling is an odd function of curvature. The related component of the shear tensor $\eta = (\pi/\kappa)\phi$ is the same whether the graphite sheet is rolled up or down, and this is as expected. Interestingly, the fact that the constant $a \neq 0$ suggests that the graphite sheet itself possesses bare anisotropy. We attribute this discrepancy to the fact that at these curvatures the carbon-carbon (C-C) bond lengths and angles are significantly distorted, even at small strains. To see this, we have extracted the spatial distribution of change in bond angles and lengths as a function of axial strain for the (8, 4) chiral SWCNT. Figure 3(a) shows the strain dependence of the three bond angles α, β, and γ [as illustrated in Fig. 3(c)] and Figs. 3(b)–3(d) are (interpolated) contour plots of the bond length distribution for $\epsilon = -2\%, 0\%$, and 2%. Evidently, the curvature itself introduces significant distortions to the hexagonal background. Bond length changes range from -0.16% to 0.12%, and the distribution is such that $\Delta a_{\text{C-C}}^{\alpha\gamma}$ is positive, $\Delta a_{\text{C-C}}^{\beta\gamma}$ negative while $\Delta a_{\text{C-C}}^{\alpha\beta}$ is relatively negligible. The bond angles α and β deviate from $2\pi/3$ by almost half a degree while γ is relatively unaffected. Note that the distortions are anisotropic and consistent with tube chirality. Since the a-SIT is now relative to an anisotropically deformed structure, it is no surprise that the behavior corresponds to a structure that possesses bare anisotropy.

Of particular interest is the anharmonicity under compression and the associated twist reversal. Careful examination of the atomic positions at ϵ_1^* and ϵ_2^* reveal that out-of-plane distortions are negligible. Hence, the effect must be restricted to the curved SWCNT surface and primarily due to a competition between bond length and angle stiffness, as well as out-of-plane π-electron resonance interactions [14]. In order to develop a continuum understanding of this effect, it is important to first understand the microscopic origin of the anharmonicity. To this end, we analyze the strain-dependent changes in bond lengths and angles, as shown in Fig. 3. Under tension, the change in the angles is monotonic [Fig. 3(a)]—α and β decrease while γ increases. Also, $\Delta a_{\text{C-C}}^{\beta\gamma}$ is positive, $\Delta a_{\text{C-C}}^{\alpha\beta}$ negative while $\Delta a_{\text{C-C}}^{\alpha\gamma}$ is negligible, consistent with a net stretch along the SWCNT axis [Fig. 3(d)]. These trends carry over to large strains as well. The compressive response is quite the opposite, in that $\Delta a_{\text{C-C}}^{\alpha\beta}$ now is positive at the expense of $\Delta a_{\text{C-C}}^{\beta\gamma}$, and $\Delta a_{\text{C-C}}^{\alpha\gamma}$ is still relatively negligible. Perhaps of more importance are the trends in bond angles. At close to the critical strain ϵ_1^*, we see a reversal in the trend in β. It starts to now decrease, while γ becomes stiffer [Fig. 3(a)] in that its rate of decrease becomes progressively smaller. The fact that this maximum in β occurs at the critical strain ϵ_1^* for this SWCNT and only under compression leads us to the conclusion that anharmonicity in the stiffness associated with bond lengths and angles start to become impor-

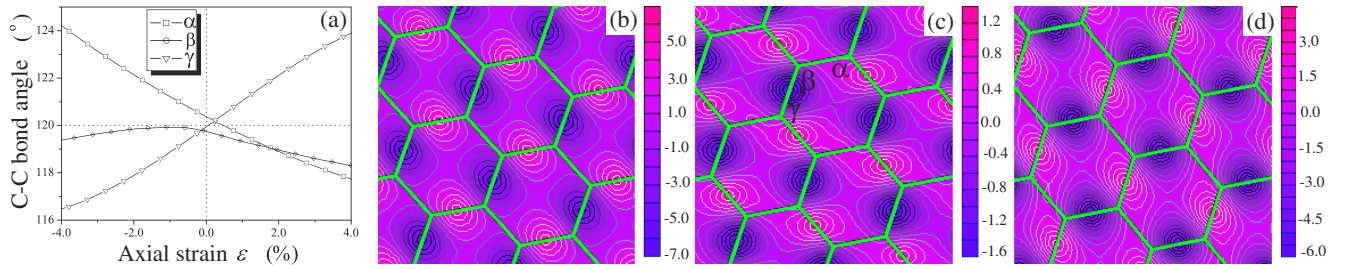

FIG. 3 (color online). (a) Strain dependence of the carbon-carbon bond angles (α, β, and γ) for the (8, 4) SWCNT. (b)–(d) Spatial distribution of the change bond lengths, for $\epsilon = -2\%$ (b), $\epsilon = 0\%$ (c), and $\epsilon = 2\%$ (d). The color scale is $\Delta a_{\text{C-C}} \times 10^3$ [red (light shading) >0 and blue (dark shading) <0], where $\Delta a_{\text{C-C}}$ is the change in bond length relative to the average value, i.e., $\Delta a_{\text{C-C}} = a_{\text{C-C}} - \bar{a}_{\text{C-C}}$. The average bond lengths are $\bar{a}_{\text{C-C}} = 1.4262$ Å, $\bar{a}_{\text{C-C}}(2\%) = 1.4381$ Å, and $\bar{a}_{\text{C-C}}(-2\%) = 1.4149$ Å.

tant at these strains, and change the competition between energy stored in bond lengths, angles, and π-electron interactions. Ongoing work includes understanding this competition using a robust microscopic framework [14], and then relating it to a macroscopic response theory.

In conclusion, we find that the a-SIT can be quite significant for technologically relevant SWCNTs, and can modify the response of CNT-NEMS devices. The static behavior shows significant deviations from continuum predictions based on harmonic strains. Ongoing work is focused on the dynamical response, as a function of strain rate and temperature (Liang and Upmanyu, [18]). The dynamical response opens up the possibility of high quality, tunable nanoscale actuators, oscillators or clocks, and nanomotors, in turn driven by electro-, thermo-, chemico-, and optico-mechanical coupling in appropriately functionalized chiral nanotubes, nanowires, and nanofilaments. The elimination of the need of electrostatic actuation of the rotation motion is a significant step forward as it facilitates fabrication of single-step, integrated CNT-NEMS devices. Pulsed voltage biases and laser fields can easily exploit the small strain a-SIT response to realize tunable rotational oscillators and regulators [15,16]. Twist reversal under compression further enriches the application set. For example, the rotational frequency can be doubled by precompressing the SWCNT to ϵ_1^* and then prescribing periodic axial strains. Applications can also be designed which exploit the reverse coupling, i.e., torsion $\rightarrow$ axial strain, and its effect on electromagnetic properties (metallic $\leftrightarrow$ semiconducting). The large-strain response (below the buckling threshold in compression) can be harnessed for molecular-manipulators and STM tips [17], to name a few. In each case, accurate predictions of the resonance frequencies combined with nanofilaments with intrinsically high CCIEA (type II BC_2N nanotubes, silicon nanotubes, for example) can further exaggerate the response [5,9].

The authors acknowledge productive discussions with D. J. Srolovitz and L. M. Mahadevan.

*Electronic address: mupmanyu@mines.edu

[1] R. H. Baughman, A. A. Zakhidov, and W. A. de Heer, Science **297**, 787 (2002).
[2] H. G. Craighead, Science **290**, 1532 (2000).
[3] S. Sapmaz, Y. M. Blanter, L. Gurevich, and H. S. J. van der Zant, Phys. Rev. B **67**, 235414 (2003).
[4] R. H. Baughman *et al.*, Science **284**, 1340 (1999).
[5] P. Poncharal, Z. L. Wang, D. Ugarte, and W. A. de Heer, Science **283**, 1513 (1999).
[6] A. M. Fenimore, T. D. Yuzvinsky, W. Q. Han, M. S. Fuhrer, J. Cumings, and A. Zettl, Nature (London) **424**, 408 (2003).
[7] S. J. Papadakis, A. R. Hall, P. A. Williams, L. Vicci, M. R. Falvo, R. Superfine, and S. Washburn, Phys. Rev. Lett. **93**, 146101 (2004).
[8] V. Sazonova, Y. Yaish, H. Ustunel, D. Roundy, T. A. Arias, and P. L. McEuen, Nature (London) **431**, 284 (2004).
[9] Y. N. Gartstein, A. A. Zakhidov, and R. H. Baughman, Phys. Rev. B **68**, 115415 (2003).
[10] D. W. Brenner, O. A. Shenderova, J. A. Harrison, S. J. Stuart, B. Ni, and S. B. Sinott, J. Phys. Condens. Matter **14**, 783 (2002).
[11] The fit is constrained to go to zero at large R, as expected for a graphite sheet. Also, the behavior of high curvature SWCNTs is an exception to the trends and excluded from the curve fit. For example, zero-strain a-SIT in the (4, 2) SWCNT lies in between that for (8, 4) and (12, 6) SWCNTs. The anomalous behavior can be attributed atomic-scale size effects due to its small radius, which results in an ill-defined surface structures.
[12] L. D. Landau and E. M. Lifshitz, *Theory of Elasticity* (Pergamon, New York, 1986).
[13] Y. Jin and F. G. Yuan, Compos. Sci. Technol. **63**, 1507 (2003).
[14] T. Lenosky, X. Gonze, and M. Teter, Nature (London) **355**, 333 (1992).
[15] R. E. Tuzun, D. W. Noid, and B. G. Sumpter, Nanotechnology **6**, 52 (1995).
[16] D. Srivastava, Nanotechnology **8**, 186 (1997).
[17] H. Dai, J. H. Hafner, A. G. Rinzler, D. T. Colbert, and R. E. Smalley, Nature (London) **384**, 147 (1996).
[18] H. Liang and M. Upmanyu (to be published).